Limnol. Oceanogr., 59(1), 2014, 115–128

doi:10.4319/lo.2014.59.01.0115

Thermal structure and variability of a shallow tropical reservoir

Zikun Xing,[1] Derek A. Fong,[2] Edmond Yat-Man Lo,[1] and Stephen G. Monismith [2,*]

[1] Division of Environmental and Water Resources Engineering, School of Civil and Environmental Engineering, Nanyang Technological University, Singapore

[2] Environmental Fluid Mechanics Laboratory, Department of Civil and Environmental Engineering, Stanford University, Stanford, California

Abstract

The structure and mixing dynamics of shallow tropical reservoirs was investigated using data collected in the Kranji Reservoir in Singapore. Water temperature data spanning a 2 month period in 2007 shows that diurnal cycles of stratification and destratification were formed in various locations in the reservoir. Temperature stratification of 0.5°C to 3.5°C was formed during the daylight hours and reduced nightly when cooling occurred. Substantial horizontal redistribution of heat was also observed between the side arms and the main body of the reservoir. The Kranji's dynamics can be summarized in terms of three physical forcing regimes: a solar radiation–dominated regime, a windy regime, and a cold inflow regime. We delineate the three physical forcing regimes by two potentially useful dimensionless numbers that quantify the relative influences of surface heating, wind stirring, and inflow buoyancy fluxes. For most of the measurement period (88% of the data record), the solar radiation–dominated regime characterized the hydrodynamics. In spite of the dominance of solar radiation in setting local stratification, it is shown that Kranji Reservoir is a three-dimensional system in which there can be significant variations in temperature in the vertical and along-reservoir directions, as determined by cold inflow events, differential heating, and reservoir releases. Moreover, the data suggest that the dynamical balance of the Kranji system is sensitive to small forcing events, with the timescales of stratification and mixing as short as a day or less.

The rapid growth of human populations in tropical regions during the last few decades has created serious environmental problems for tropical lakes and reservoirs, most notably eutrophication (Nilssen 1984; Crisman and Streever 1996; Parinet et al. 2004). Thus, management of these tropical inland waters requires a thorough understanding of thermal stratification and mixing processes operating in them because stratification and mixing are critical for primary production (Nilssen 1984; Ruardij et al. 1997; Talling 2001). However, compared to the many studies of temperate lakes, studies of the physics of tropical lakes and reservoirs are relatively few (Boon 1996; Lewis 2000; MacIntyre et al. 2002).

Tropical lakes are generally characterized by higher levels of, and weaker seasonal variations in, solar radiation than are experienced by temperate lakes throughout the year except for periods with high cloud cover (Lewis 1987; Talling and Lemoalle 1998; Gunkel and Casallas 2002). Consequently, water temperature in tropical lakes is generally warmer as a result of larger solar radiation. The higher solar radiation combined with low variations in solar radiation throughout the year in tropical lakes implies that the differences between surface and bottom temperatures in tropical lakes are generally lower than in temperate lakes. The Schmidt stability (Idso 1973) of the water column is generally lower than in temperate lakes with comparable sizes, even though the thermal expansion coefficient varies with temperature (Lewis 1987). The stratification cycle and mixing dynamics are also appreciably different for deep and shallow tropical lakes. Many earlier studies on tropical limnology focused on deep rather than shallow lakes (Crisman and Streever 1996). Deeper tropical lakes (i.e., those with an average depth of approximately 10 m or greater) tend to be warm monomictic, i.e., they mix once per year (normally in winter) and are stably stratified for the rest of the year (Hutchinson and Löffler 1956; Lewis 1983, 2000). Furthermore, diurnal stratification is superimposed upon the deeper seasonal stratification (Lewis 1973; Talling and Lemoalle 1998). In contrast, shallow tropical lakes may achieve complete mixing of the whole water column multiple times every year, possibly even mixing diurnally (Lewis 2000; Talling 2001; Antenucci et al. 2013). It should be noted that some shallow temperate lakes, such as Clear Lake in California, can experience complete mixing with periodic stratification and destratification events on a diurnal timescale during the early summer (Rueda and Schladow 2003; Rueda et al. 2003). Therefore, some of the physics described in this study may be relevant to shallow temperate lakes during certain times of the year.

Talling and Lemoalle (1998) reviewed mixing dynamics and water temperature cycles in tropical lakes, focusing on deeper tropical lakes and annual cycles of water temperature. Due to the higher radiative heating and lower stability, the thickness of the diurnal mixed layer in tropical lakes is more variable than that of temperate lakes (Lewis 1987). The diurnal thermocline formed during the strong heating period deepens in the night. Convective motions between the side arms and the deeper main body of the lake, arising from the different rates of daytime heating and nighttime cooling, may also contribute to a large degree to the thermal structure and diurnal (de)stratification cycles

* Corresponding author: monismith@stanford.edu

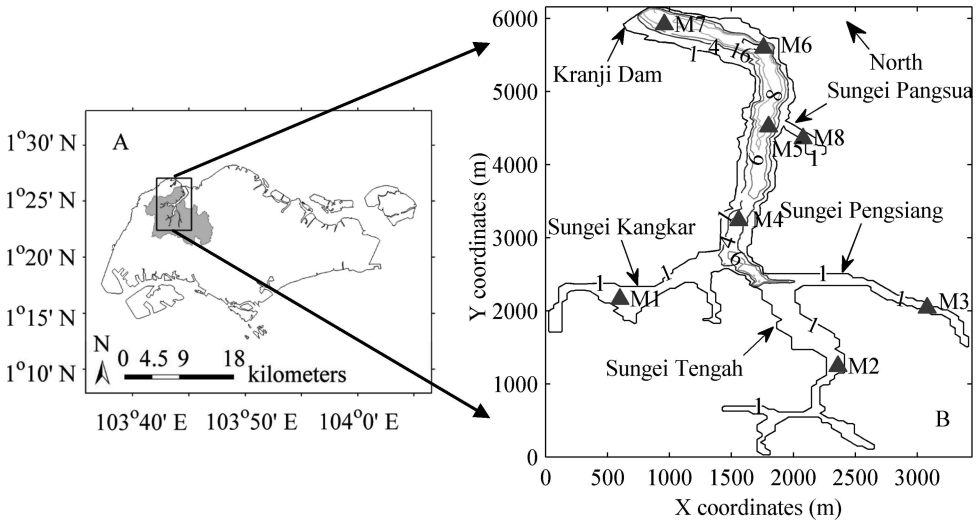

Fig. 1. (A) Locator map of Kranji Reservoir in Singapore, showing the water body and its catchment. (B) Contour map of Kranji Reservoir with experimental mooring stations in April to June 2007, showing the four important tributaries making the inflow, the Kranji dam, and locations of the field deployment stations in 2007: thermistor chains (M1 to M8) and ADCP (M4, M5, and M6).

(Monismith et al. 1990). In addition, shallow lakes can have notable horizontal variations in thermal structure due to spatial differences in the depth of wind mixing (MacIntyre and Melack 1995; MacIntyre et al. 2002).

The present study focuses on the thermal structure and mixing dynamics of Kranji Reservoir, a shallow tropical reservoir located in Singapore (Fig. 1). A description of Kranji Reservoir and the field experiments carried out are presented in the Methods section. The Results section focuses on the data collected during a field deployment in 2007 and presents observed diurnal cycles of thermal stratification and horizontal temperature gradients in the reservoir. The Discussion section describes how Kranji's dynamics can be summarized in terms of three physical forcing regimes. The physics of each regime is further illustrated by detailed examination of short periods in the data set that fall within each of the three regimes. Typically, the hydrodynamics of lakes and reservoirs are described and classified in terms of two parameters, i.e., the Lake number and the Froude number, which assume the presence of a seasonal thermocline. However, for shallow tropical reservoirs where wind stress, surface heating, and inflows interact on different timescales, it is likely that they are either not necessarily sufficient to describe the thermal cycling or not applicable due to the lack of a seasonal thermocline. In the Discussion section, we have introduced two new dimensionless numbers that can better characterize the stratification dynamics. The implications of this study are presented at the end of the Discussion section.

There are few in-depth studies on the thermal structure and variability of a shallow tropical reservoir in response to forcing events on timescales as short as within 1 d. A related recent study by Antenucci et al. (2013) noted the diurnal heating and cooling pattern for Marina Reservoir, another shallow tropical reservoir in Singapore, in the context of analyzing dissolved oxygen, but it did not provide detailed analysis of its thermal structure.

Methods

Study site—Kranji Reservoir (1°25′N, 103°43′E) is located at the northwest corner of Singapore Island. It is a former river, which was dammed at its mouth in 1972 to form a freshwater storage reservoir. The total area of the Kranji catchment is about 5.6×10^7 m^2; the surface area of Kranji Reservoir has been estimated to be about 3.0×10^6 m^2 and the maximum volume is 1.6×10^7 m^3. The length of the main channel of Kranji Reservoir is about 4 km, with maximum depth of about 20 m and average depth of about 5 m. It is one of the water supply reservoirs in Singapore. There are four major tributaries flowing into Kranji Reservoir: Sungei Kangkar, Sungei Tengah, Sungei Peng Siang, and Sungei Pang Sua. Sungei Pang Sua was diverted into Kranji Reservoir at the end of 2005. Kranji Reservoir is almost entirely fed by dry weather flow and storm runoff from the four tributaries and direct precipitation on the reservoir. The outflow of the reservoir includes releases at the Kranji Dam and pumping to water works. A map of Kranji Reservoir and its catchment is shown in Fig. 1. Among other features, measured extinction depths for solar radiation are on the order of 1 m; this is typically associated with the relatively high algal biomass (Gin and Gopalakrishnan 2010).

Field deployment and data collected—A field deployment consisting of thermistor chains using Sea-Bird SBE 39 temperature loggers and two upward-looking 1200 kHz and one upward-looking 600 kHz Teledyne RD Instruments (RDI) acoustic Doppler current profilers (ADCP) was carried out in Kranji Reservoir from 10 April (day of the year [DOY] 100) to 14 June (DOY 165) in 2007; this

Table 1. Details of instruments used at each mooring site during field deployment in 2007.

Moorings	Depth (m)	Instruments	Details	Sampling interval	Estimated accuracy
M1	1.7	Thermistor	1 mab	30 s	0.002°C
M2	1.7	Thermistor	1 mab	30 s	0.002°C
M3	1.1	Thermistor	0.5 mab	30 s	0.002°C
M4	6.1	Thermistor chain	1,2,3,4,5 mab	30 s	0.002°C
		1200 KHz RDI ADCP	0.72–5.32 mab; 0.2 m bins	4 min	0.64 cm s^{-1}
M5	8.4	Thermistor chain	1,2,3,4,5,6,7 mab	30 s	0.002°C
		1200 KHz RDI ADCP	0.72–6.52 mab; 0.2 m bins	4 min	0.64 cm s^{-1}
M6	13.3	Thermistor chain	2,4,6,7,8,9,10,11,12 mab	30 s	0.002°C
		600 KHz RDI ADCP	1.61–11.11 mab; 0.5 m bins	4 min	0.46 cm s^{-1}
M7	7.9	Thermistor chain	1,3,5,6 mab	30 s	0.002°C
M8	2.3	Thermistor chain	0.5, 1.5, 2.3 mab	30 s	0.002°C

mab, meters above the reservoir bottom.

paper focuses primarily on the water temperatures and velocities measured during this period. The locations of the eight mooring stations (labeled as M1–M8) and the instruments deployed are also shown in Fig. 1, and a summary of the instrument details is provided in Table 1. During this field deployment period, a meteorological station located near M5 was operating (hereafter, referred to as the Met Station). The station recorded air temperature, relative humidity, wind speed and direction, shortwave radiation, and rainfall at 15 min intervals using sensors installed at 1.5 m above water surface (*see* table 3 of Xing et al. [2012] for instrument details). Unfortunately, there was a short gap of about 10 d in the data recorded at the station from 06 May (DOY 126) to 15 May 2007 (DOY 135) due to an equipment malfunction. The meteorological data with the exception of the rainfall data were filtered with a fourth-order low-pass Butterworth filter with a cutoff timescale of 2 h.

Tributary inflows calculation—To compute the daily total tributary inflow volume, we used the well-established hydrological and hydraulic model XP Stormwater and Wastewater Management Model (XP Software 2005; http://www.xpsoftware.com/), which was established and calibrated over both single and continuous storm flow events to predict the direct runoff from the four main catchments in the Kranji Catchment (Tan et al. 2008). As discussed in Xing et al. (2012), inflow computed using daily rainfall as inputs compared well with the measured daily dam outflow of Kranji Reservoir.

Results

Meteorological observations—The meteorological measurements during the field deployment period are shown in Fig. 2. Diurnal patterns of wind speed, solar radiation, air temperature, and relative humidity were noted. Wind speed had an average value of 1.27 m s^{-1} and a maximum value of 6.64 m s^{-1}. Wind forcing was generally higher in the afternoon, when it came from the northeast, and lower in the night. For most of the days, solar radiation peaked between 500 W m^{-2} and 1000 W m^{-2}. Air temperature underwent a cooling period from DOYs 116 to 120 and stayed low for a few days; this was followed by a gradual warming. The relative humidity peaked near 100% daily and averaged 84%. There were a number of rainfall events, particularly over DOYs 116 to 120 (*see* Fig. 2F), with the largest event in terms of runoff volume occurring on DOY 116. These events will be shown below to drive significant vertical and horizontal stratification.

Diurnal cycles of thermal stratification—Time series of water temperature at surface, middle, and bottom depths at M4 (the junction of three tributaries) and at M6 (the deepest mooring station along the main channel of Kranji Reservoir) are plotted in Fig. 3A,C for the field deployment period. The temperature of the surface water exhibited a clear diurnal cycle, and the temperature of the middle and bottom water changed more slowly, over a period of several days. Periodic stratification and destratification occurred diurnally. Several cold inflow events are present in this record, with the largest single event occurring on DOY 116, after which the water column remained stratified for about 3 d before complete mixing resumed on a diurnal basis (for detailed structure of temperature and flow, *see* fig. 3 of Xing et al. 2012). Early in the record, the lake was well mixed, after which it warmed up by approximately 1°C before being cooled down by the cooler air temperature (*see* Figs. 2D, 3A,C) and cold storm inflows during DOYs 113 to 117. The water column was then warmed again and was well mixed again by DOY 119.

Differences (ΔT) between the surface and the bottom temperatures at M4 and M6 are plotted in Fig. 3B,D. Diurnal cycles of stratification and destratification can be observed at both the locations. Generally, stratification (defined here by ΔT) of 0.5°C to 3.0°C formed during the daylight hours and reduced nightly when cooling occurred. The maximum stratification observed during the deployment occurred at M4 during the largest inflow event of the record, when cold inflows from tributaries plunged into the deeper part of the junction of these tributaries and increased the stratification.

Horizontal temperature differences—Horizontal temperature differences at 1 m and 5 m below the water surface along the main channel of the reservoir were substantial and comparable to vertical variations (Fig. 4A,B). There

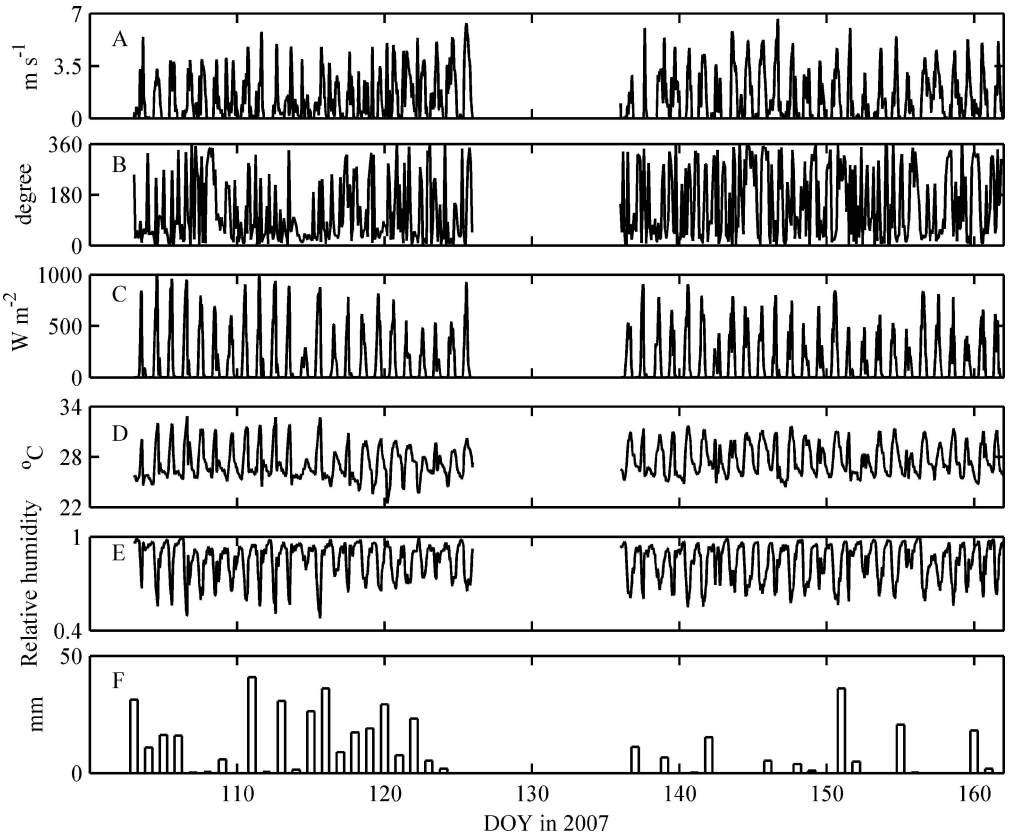

Fig. 2. Meteorological data of (A) wind speed, (B) wind direction, (C) shortwave radiation, (D) air temperature, (E) relative humidity, and (F) rainfall depth. The time interval of meteorological data is (A, C–E) every 15 min, (B) every 2 h, and (F) daily. The blank area between DOYs 126 to 135 of 2007 indicates the period when equipment malfunction happened.

were also significant temporal variations: differences were generally greater near the water surface (1 m below) than near the bottom (5 m below), with the exception of the cold inflow event from DOY 113 to DOY 117, in which the cold inflows from the tributaries plunged into deeper parts of the junction (M4) and formed the large horizontal temperature difference at the deeper depths. As expected from past observations (Monismith et al. 1990), water temperature changes in the shallower arms during daytime heating and nighttime cooling were larger than in the deeper main channel (Fig. 4C,D). Thus, we expect that thermally driven horizontal exchange should be a key transport mechanism in Kranji.

Observed behavior: three types of days—We have found that Kranji's thermal structure varied during different days and that, as shown below, there are generally three types of days describing the different stratification and mixing dynamics, specifically, solar radiation–dominated days, windy days, and cold inflow days.

For the solar radiation–dominated days, the incoming solar radiation was typically large during the day, and strong vertical stratification formed in the afternoon. For example, on DOY 110, the reservoir was nearly well mixed in the early morning. Due to solar radiation during the day, the reservoir became vertically stratified in the afternoon, developing a shallow surface layer about 2 m thick (*see* Fig. 5D). Much like the diurnal mixed layer discussed in Imberger (1985), this layer deepened nearly to the bottom at night due to surface cooling (not shown).

Vertical temperature profiles and the current velocities at M4, M5, and M6 for DOY 110 are also shown in Fig. 5A–C. In the morning (09:00 h to 12:00 h), the lake exhibited little vertical stratification, the wind was as low as 2.5 m s^{-1}, and the velocities at all three stations were insignificant. The vertical stratification started to build up (12:00 h to 15:00 h) and peaked in the late afternoon (15:00 h to 18:00 h). There were also notable horizontal temperature differences ($\sim$ 1.0°C) in the surface waters between the shallower stations (M4 and M5) and the deeper station (M6), as shallower regions were expected to have larger temperature changes than deeper locations during the daytime heating (Monismith et al. 1990). The wind coming from the dam direction peaked at 5 m s^{-1} in the late afternoon as well. Both the horizontal temperature differences and the stronger wind led to a significant flow ($\sim$ 0.05 m s^{-1}) of the surface waters from the dam to the junction of the tributaries, with a return flow in the middle depth that was enhanced by tributary inflows.

For the windy days, strong winds mixed the waters in the surface layer and deepened it. The stratification of the water column was dominated by the wind mixing instead of the net heat flux. As an example of a windy day, the time evolution of the Kranji temperature field of DOY 125 is

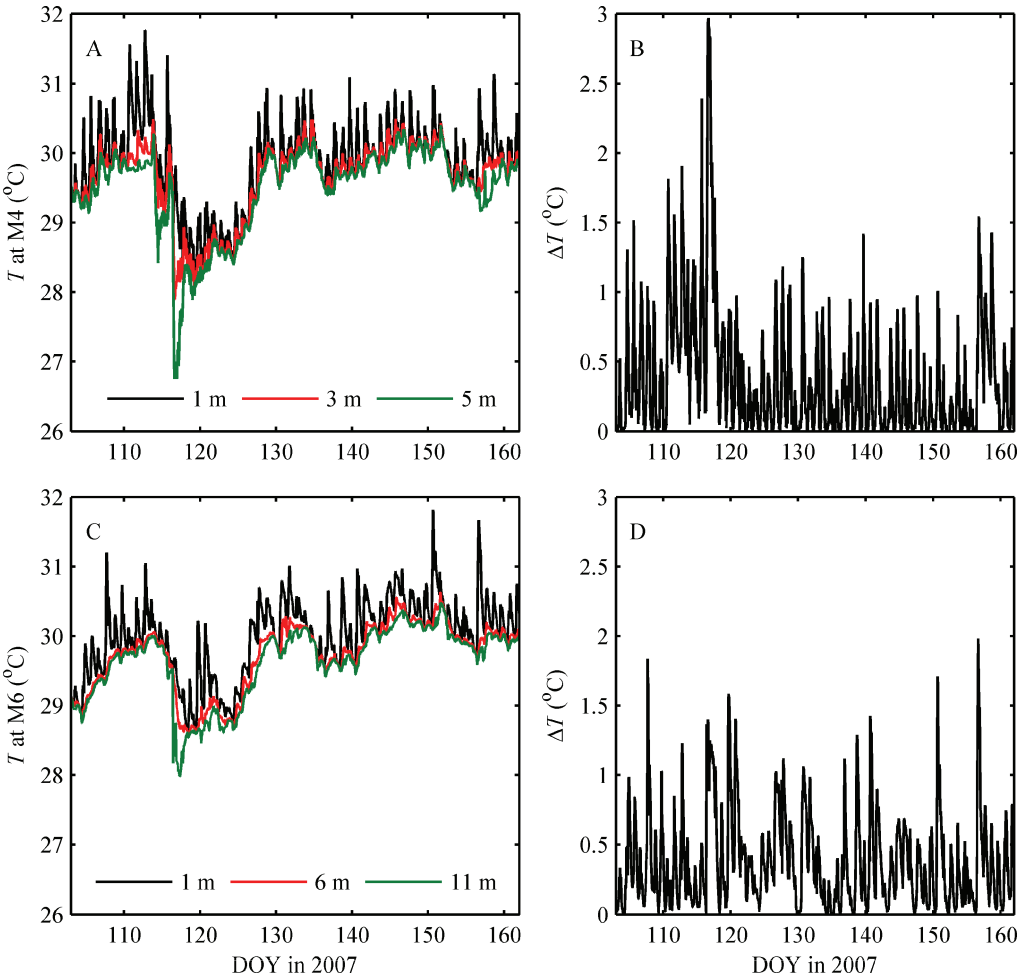

Fig. 3. Water temperatures at different depths of (A) M4 at 1 m, 3 m, and 5 m below surface and (C) M6 at 1 m, 6 m, and 11 m below surface; and thermal stratification ($\Delta T = T_{top} - T_{bottom}$) at (B) M4 and (D) M6 for the field deployment period from DOYs 103 to 162 of 2007.

shown in Fig. 6D. In the afternoon, strong wind mixing in the surface layer prevented the formation of stable vertical stratification in the reservoir.

Vertical temperature profiles and the current velocities at M4, M5, and M6 on DOY 125 are also shown in Fig. 6. Horizontal temperature differences remained comparable to vertical temperature differences (in terms of ΔT) between the shallower stations (M4 and M5) and the deeper station (M6) during 09:00 h to 18:00 h. Due to the varying cross-reservoir topography, the wind-driven flow near the surface was upwind in the deeper center channel of Kranji Reservoir, as measured by ADCPs; we hypothesize that a reverse flow develops downwind in the shallower side regions (not measured), corresponding to the wind-driven flow pattern shown in Fischer (1976). The mid–water column flows at the moorings in the main channel were toward the tributaries, suggesting a baroclinically dominated flow. The complex wind- and density-driven flow in the presence of varying topography is beyond the scope of this study.

The horizontal temperature difference in the surface waters between shallower and deeper stations is reduced from 09:00–12:00 h to 12:00–15:00 h. However it was increased by 0.05°C during 15:00–18:00 h. This is due to weak solar radiation and strong wind mixing in this period, when the vertical stratification in the shallower region reduced and the surface temperature dropped.

For the cold inflow days, an appreciable amount of cold inflow arising from large rainfall events plunged into the lower layers of the water column and increased the stratification. For example, on DOY 116, from 11:00 h in the morning, large cold inflows from tributaries plunged into the deeper part of the junction (M4) and increased ΔT to as high as 3.0°C at M4 (Fig. 7). Vertical ΔT_{max} in the main channel of the reservoir reached 1.73°C, which was the largest value of ΔT_{max} observed during the 2 month field deployment period. Relatively large vertical stratification and horizontal temperature gradients were maintained during the night of DOY 116 and throughout DOY 117. On DOY 117 the daily averaged shortwave solar radiation $\overline{Q}_{sw}$was 127 W m^{-2} (not shown). With increased radiation and smaller cold inflow during DOY 117, a surface layer of around 2 m formed in the afternoon, such that the system reverted to behaving like a one-dimensional

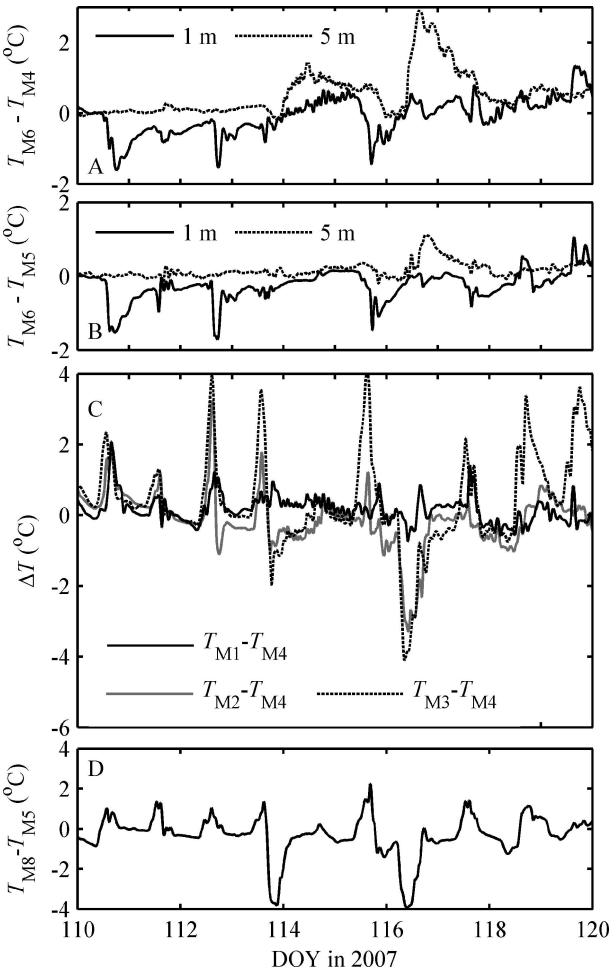

Fig. 4. (A) Horizontal temperature differences from M6 to M4 at 1 m and 5 m below surface, (B) horizontal temperature differences from M6 to M5 at 1 m and 5 m below surface, (C) horizontal temperature differences of surface water temperatures from the three tributaries (M1, M2, and M3) to the junction (M4), and (D) horizontal temperature differences of surface water temperatures from the Sungei Pangsua channel to its inlet in the main channel (M5) for the field deployment period from DOYs 103 to 162 of 2007.

system after 17:00 h of DOY 117. However, the water column was still cold in DOY 117, and it took 3 d to recover (*see* Fig. 3).

Vertical temperature profiles and the current velocities at M4, M5, and M6 are shown in Fig. 7 for DOY 116. In the early morning (06:00 h to 09:00 h), the lake exhibited little vertical stratification, and the wind was as low as 1.0 m s^{-1}. The cold inflow entered the main channel with surface flow as large as 0.1 m s^{-1} at M4, about 0.05 m s^{-1} at M5, and near zero at M6. The vertical stratification started to build up from 09:00 h to 12:00 h, and the velocity at the surface of both M4 and M5 reached 0.1 m s^{-1}. The cold inflow plunged into the deeper part of M4, and the velocity at 2 to 4 m below the surface exceeded the surface velocity of M4. From 12:00 h to 15:00 h, large horizontal temperature differences formed in the deeper waters between M4 and M6. Thus, velocity up to 0.1 m s^{-1} at the depth of 4 m under the surface and a negative surface velocity of -0.04 m s^{-1} were observed. Strong vertical stratification peaked at 3.0°C at M4 from 15:00 h to 18:00 h, when the surface temperatures at the three stations were close to each other, whereas horizontal temperature differences between M4 and M6 peaked at near 3.0°C at 5 m below the surface. The substantial horizontal temperature differences during this period led to a velocity profile at M4 with a negative velocity of -0.06 m s^{-1} at the surface waters and 0.10 m s^{-1} at 5 m below the surface. In the afternoon, the wind ($\sim$ 2.5 m s^{-1}) blowing from the dam may have also contributed to the surface flow; however, the vertical wind mixing was not sufficient to deepen the diurnal mixed layer at the stations.

Discussion

We show below that Kranji's thermal dynamics, characterized in terms of three fundamental physical forcing regimes, can be determined by the buoyancy of inflows and by surface forcing due to winds and surface heat exchanges.

Traditionally, reservoir dynamics have been characterized in terms of two parameters, the Lake number, L_N (Imberger and Patterson 1990), and the Froude number, Fr, given by the expressions:

$$L_N = \frac{gS_t(1-z_T/z_m)}{\rho u_*^2 A_s^{3/2}(1-z_g/z_m)} \quad (1)$$

and

$$Fr = \frac{Q}{A_c(g'H)^{1/2}} \quad (2)$$

where S_t is the Birge stability (Idso 1973), z_T is the height of the thermocline, z_m is the height of the center of mass, z_g is the height of the center of volume, A_s is the surface area of the reservoir, u_* is the shear stress of the wind (drag coefficient of 1.3×10^{-3} is used to compute u_*), Q is the inflow flow rate, $g' = \alpha \Delta T_0 g$ is the effective reduced gravity of the inflow defined using the temperature contrast between reservoir and inflow of ΔT_0, α is the thermal expansion coefficient for a linear equation of state, A_c is the cross-sectional area, and H is the mean depth of the reservoir.

L_N measures the likelihood of upwelling and concomitant longitudinal variations in temperature, whereas Fr is taken to represent the production of similar temperature variations by inflows (Imberger and Patterson 1990). When $L_N < 1$, upwelling is likely; whereas, when $L_N > 1$, stratification dominates the forces introduced by surface wind energy and little seiching of the seasonal thermocline is expected (Robertson and Imberger 1994). Likewise, when $Fr < 1$, inflows are weak and the reservoir stratification remains vertical.

L_N is generally used when there is seasonal thermocline, and it assumes that wind is the dominating force for mixing while neglecting the inflow and outflow. However, in a shallow tropical reservoir system like Kranji Reservoir, a seasonal thermocline does not exist; and, as our analysis shows, the cold inflows will increase the stratification, which was not included in the calculation of L_N. Thus L_N cannot fully describe the dynamics in shallow

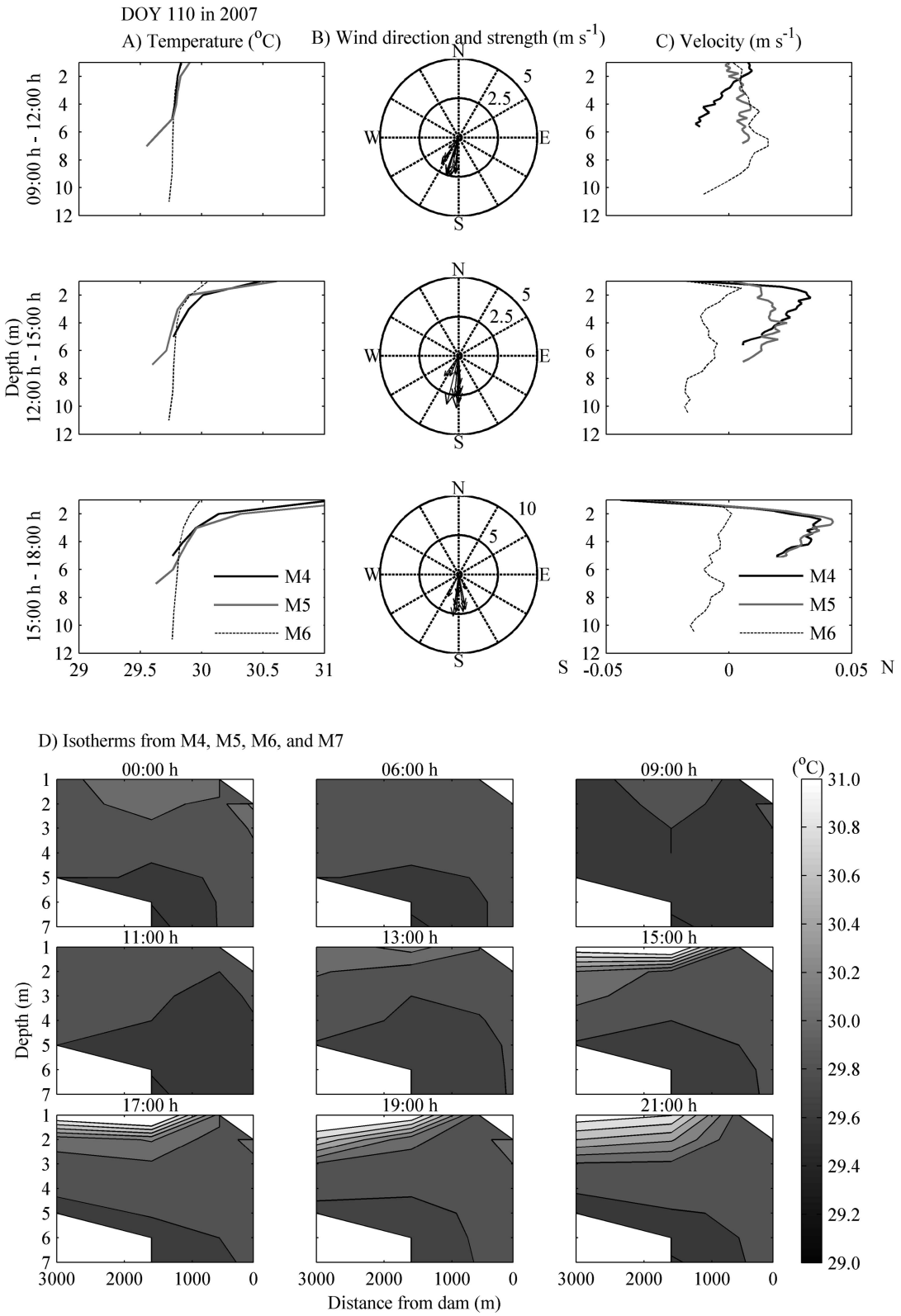

Fig. 5. DOY 110 in 2007. (A) Water temperature at M4, M5, and M6 averaged over 3 h. (B) Wind direction and strength during the 3 h, with the arrows pointing in the direction the wind is blowing. (C) Velocity along the main channel at M4, M5, and M6 averaged over 3 h on the same day, with the positive direction defined as along the main channel and toward the Kranji dam. (D) Isotherms, plotted by interpolating water temperature measured by thermistors from 1 m to 7 m in the four mooring stations (M4, M5, M6, and M7) in the main channel. The interval between contour lines is 0.2°C. The *x*-axis is the distance from dam in meters and the *y*-axis is the depth from water surface in meters.

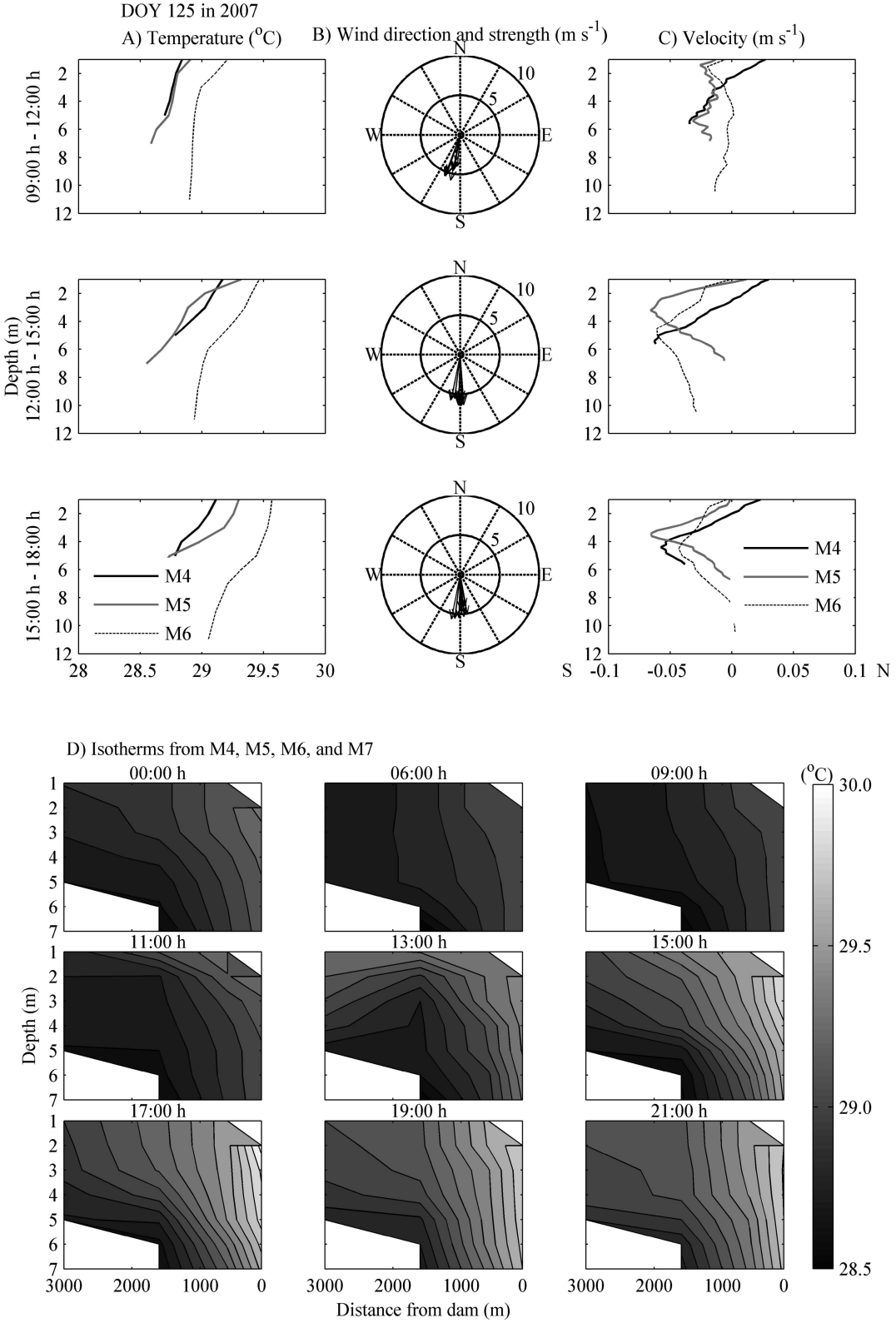

Fig. 6. DOY 125 in 2007. As in Fig. 5.

tropical lakes and reservoirs. As for the Froude number, it decreases when the temperature contrast between reservoir and inflow increases. However, as shown in the cold inflow days of the Results section, a large ΔT_0 will increase the stratification in the reservoir. In addition, the *Fr* (calculated below in Fig. 8) is much less than 1 all the time, showing that inflows are weak, which is not the case here.

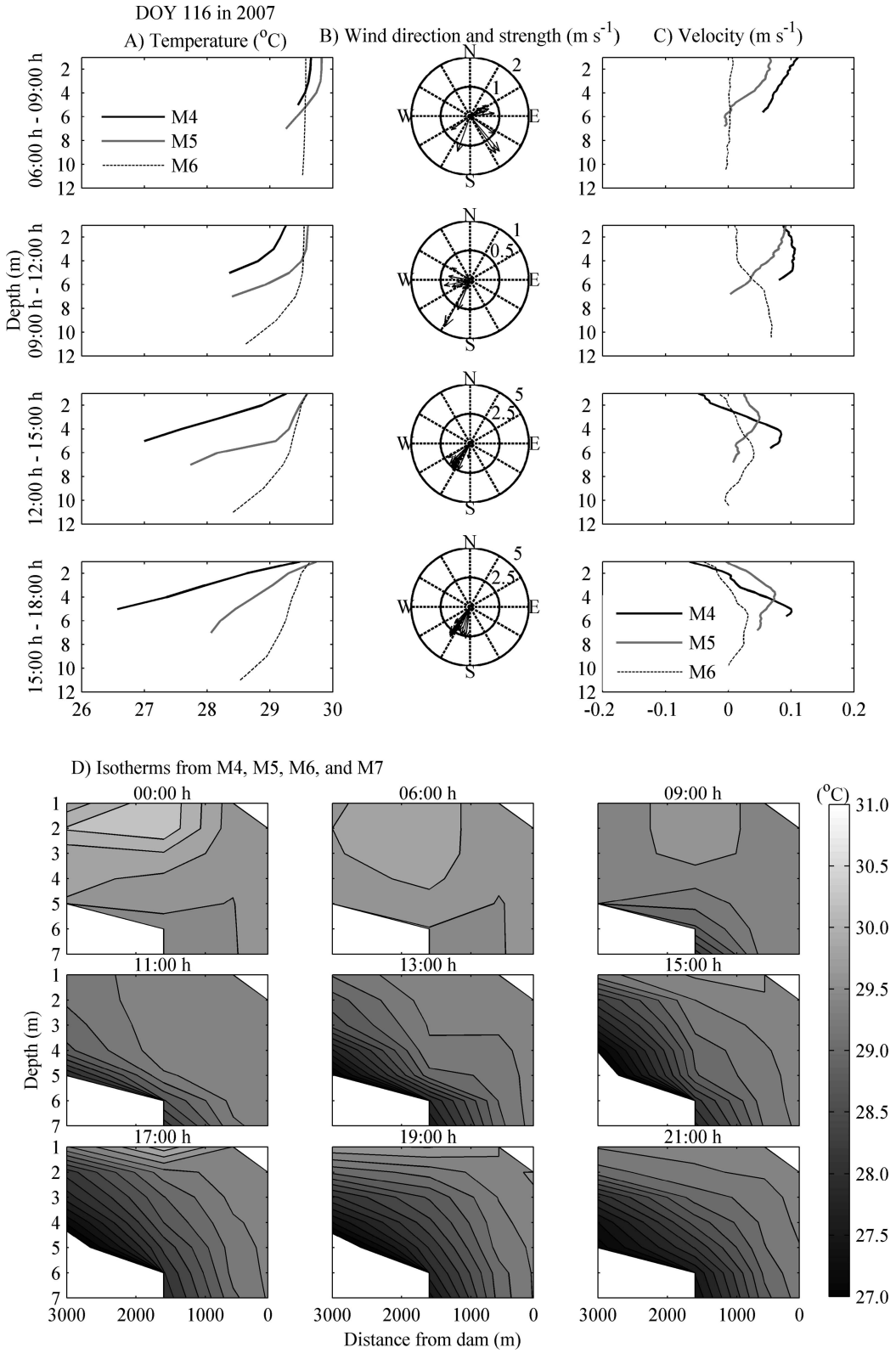

Fig. 7. DOY 116 in 2007. As in Fig. 5.

As an alternative, we next develop two new dimensionless numbers of I_{IW} and I_{WB} incorporating the competing forces of wind stress, surface heating, and inflows. I_{IW} is associated with the stratifying effect of the inflow in the face of wind mixing; I_{WB} is a measure of the importance of wind to surface heat mixing processes. As shown below, they can be used to effectively characterize the stratification dynamics of the Kranji.

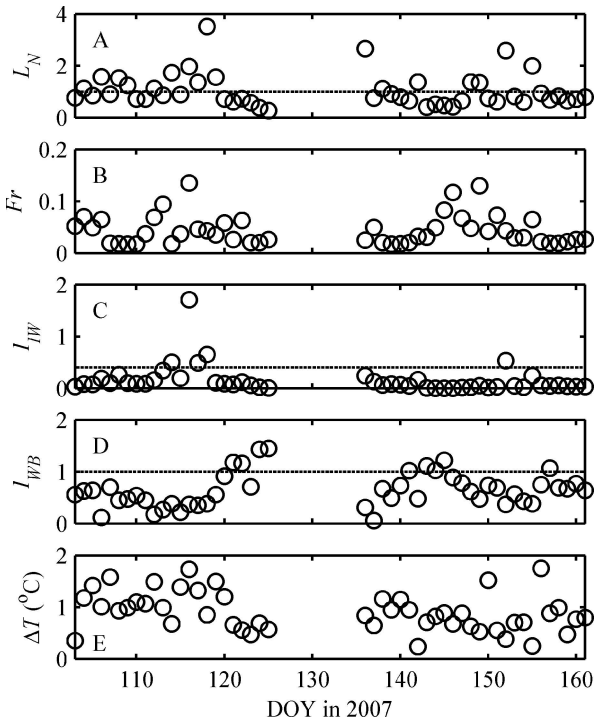

Fig. 8. Daily average dimensionless parameters of (A) Lake number, (B) Froude number, (C) I_{IW}, (D) I_{WB}, and (E) thermal stratification (ΔT) for Kranji Reservoir for the field deployment period from DOYs 103 to 162 of 2007.

To evaluate the relative strength of buoyancy flux associated with cold inflows and wind stress in terms of energy fluxes, we proceed as follows. The buoyancy flux of the tributary inflows is defined by $B = g'Q$, where g' is the effective reduced gravity of the inflow and Q is the inflow rate (Fischer et al. 1979). The effect of wind mixing, expressed in the same units, is $(u_*^3/h)A_s$, i.e., expressed as a depth-averaged turbulent kinetic energy input rate (*see* Pope 2000, p. 88), where h is the depth of surface mixed layer. Thus, a dimensionless parameter that represents the relative balance of inflow-induced stratification and its mixing by wind stresses is

$$I_{IW} = \frac{Bh}{u_*^3 A_s} \tag{3}$$

We expect that, when $I_{IW} << 1$, wind mixing eliminates stratification induced by the inflow; whereas, when $I_{IW} >> 1$, wind mixing is weak and stratification should be directly related to inflows.

The second critical parameter is the strength of wind mixing relative to the effects of surface heat fluxes, including radiation. As before, the surface turbulent kinetic energy flux is given by u_*^3/h, whereas the surface buoyancy flux is equal to

$$B_s = -\alpha g \tilde{H}/\rho c_p = u_f^3/h \tag{4}$$

where u_f stands for the velocity scale associated with the daytime heating, $\tilde{H}$ is the surface heat flux (positive when cooling), and c_p is the heat capacity at constant pressure (Imberger 1985). As discussed in Fischer et al. (1979), the buoyancy flux can be expressed in terms of a velocity that will be positive for cooling and negative for heating. Since the principal concern of our analysis is the dynamics of daytime stratification, we can then define the competing effects of heating and wind mixing using the ratio of these two velocities:

$$I_{WB} = -\frac{u_*}{u_f} \tag{5}$$

This ratio is similar to the ratio of the Monin–Obukhov length, which is the height at which wind stirring balances surface heat fluxes in terms of energy, to the mixed layer depth (Imberger 1985). When $I_{WB} > 1$ we would expect wind mixing to dominate stratification production, whereas if $I_{WB} < 1$ and positive, stratification will develop due to radiative heating.

In summary, four parameters may potentially be used to describe the response of the lake temperature field to physical forcing; daily averaged values (averaging 24 h, assumed to be zero during the lake cooling period) of all four parameters are plotted in Fig. 8.

For much of the observational period, daily averaged values of $L_N \sim 1$ or less, implying that longitudinal variations in thermal structure due to upwelling should be common. As we will discuss below, this is not the case, probably because the stratification, created by surface heating in the daytime and destroyed by the convective cooling in the nighttime, occurs at a timescale shorter than what would constitute the period for first-mode internal seiching, T_i. The latter is estimated using the expression for a two-layer stratification given in Spigel and Imberger (1980) as

$$T_i = \frac{2L}{c_i} = 9.4 \times 10^4 \text{ s} = 26.1 \text{ h} \tag{6}$$

where

$$c_i = \sqrt{\frac{g' h_1 h_2}{h_1 + h_2}} = 0.07 \text{ m s}^{-1} \tag{7}$$

and $h_1 = 2$ m, $h_2 = 6$ m, $L = 3$ km, and $g' = 0.003$ m^2 s^{-1}. Thus, T_i is somewhat greater than a day, whereas the stratification changes diurnally.

Alternatively, the horizontal adjustment timescale of baroclinic velocities induced by longitudinal temperature gradients can be estimated using the "long box" analysis presented in Cormack et al. (1974) as

$$U_{\max} \approx 0.01 \frac{\alpha g (\partial T/\partial x) H^3}{\nu_t} \approx 0.1 \frac{\alpha g (\partial T/\partial x) H^2}{u_*} \tag{8}$$

where, for wind-mixed conditions, we have assumed $\nu_t \approx 0.1 H u_*$. Using appropriate values of these parameters, e.g., $\partial T/\partial x \approx 2 \times 10^{-4}$ °C m^{-1} and $u_* \approx 5 \times 10^{-3}$ m s^{-1}, gives $U_{\max} \approx 4$ mm s^{-1}, implying a horizontal adjustment timescale for the length of the reservoir of approximately 8.5 d. Thus, the reservoir also adjusts more slowly to these variations than they are created or destroyed. As suggested earlier, the dynamics studied here might also pertain to

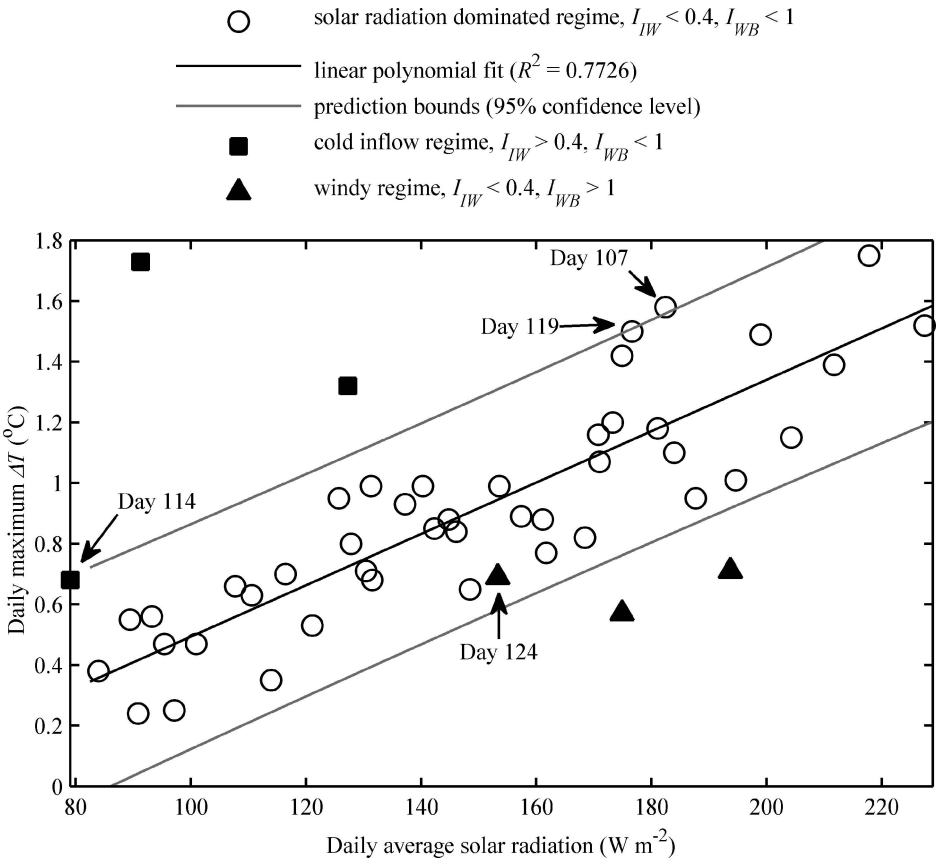

Fig. 9. Comparison of daily maximum vertical temperature difference (ΔT) and daily average solar radiation (R^2 of the linear regression is 0.7839, the calculation of which excluded the days in the cold inflow regime and the windy regime), showing three physical forcing regimes, the criteria of each regime, and the exceptions.

shallow temperate lakes in the summer, when stratification is sometimes removed on a diurnal basis.

Likewise, *Fr* is generally small and within the range of 0 to 0.2. In the usual context, this implies that inflows do not perturb the largely vertical stratification (Imberger and Patterson 1990). Finally, the two parameters we introduced above, I_{IW} and I_{WB}, show that, for most of the record, wind mixing is weaker than heating and that inflows are also generally weak; both have a few notable exceptions that we discuss below.

The utility of I_{IW} and I_{WB} can be seen by plotting the daily maximum vertical ΔT (averaging the four mooring stations located in the reservoir main channel) as a function of daily average solar radiation. This was done for all days of the deployment period from DOYs 103 through 162 in 2007, except for days 126 to 135, when solar radiation data measured by the Met Station were not available. The stratification in the reservoir was linearly related to the average solar radiation during the day (Fig. 9). This is to be expected since, in the absence of other effects (e.g., inflows or cooling), conservation of heat implies that

$$\Delta T_{\max} = -\frac{1}{\rho c_p h_h}\int Q_{sw}\,dt_{\text{heat}} = -\frac{T_{\text{day}}\,\overline{Q}_{sw}}{\rho c_p h_h} \qquad (9)$$

Here, h_h is the thickness (m) of the near-surface layer, where the shortwave radiation in W m^{-2} is absorbed and through which its effects are mixed. T_{day} is 86,400 s, and t_{heat} is taken to be the daylight hours, i.e., 43,200 s (07:00 h–19:00 h). Linear regression of the data in Fig. 9 gives

$$\Delta T_{\max} = \beta(\,\overline{Q}_{sw} - \gamma) \qquad (10)$$

Here, β equals 8.6×10^{-3} K m^2 W^{-1} and γ equals 42 W m^{-2}. The offset γ implies that the net effect of longwave radiation and latent and sensible heat fluxes averages about -42 W m^{-2} (cooling), whereas the slope β implies that $h_h \approx 2.4$ m.

Uncertainties exist in deriving the linear regression line shown in Fig. 9. The main uncertainties are from the neglect of horizontal heat redistribution mitigated with the use of an average ΔT from the four mooring stations along the reservoir main channel and the neglect of spatial variability in the solar radiation as measured by the single Met Station. Prediction bounds of 95% confidence level are plotted in Fig. 9 to take into account the uncertainties of the linear regression equation. Daily average dimensionless numbers are also plotted in the I_{IW}–I_{WB} plane together with the boundaries of different regimes (*see* Fig. 10).

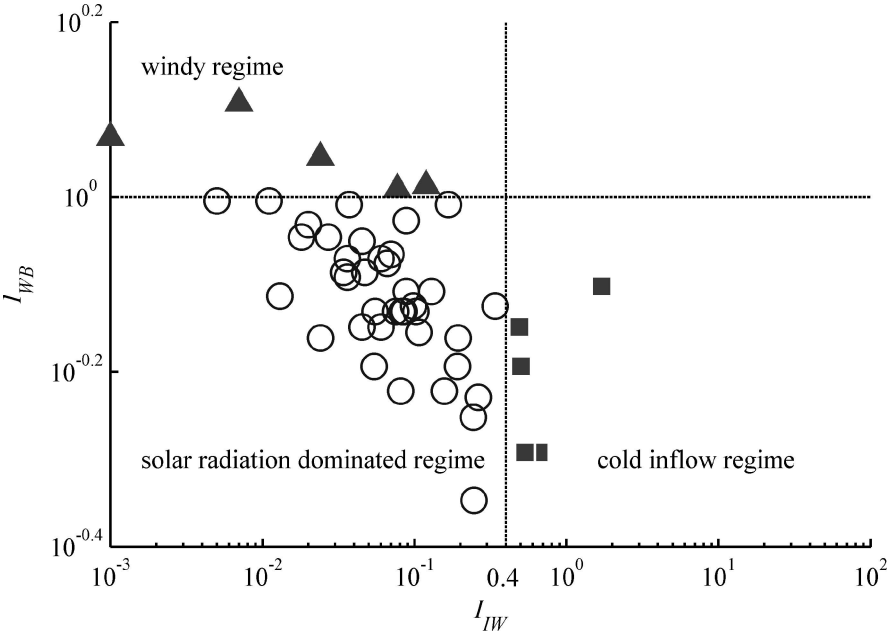

Fig. 10. Daily average I_{WB} vs. I_{IW} for the field deployment period from DOYs 103 to 162 of 2007 in the I_{IW}–I_{WB} plane, which shows boundaries of different regimes.

The data shown in Figs. 9 and 10 illustrate three different forcing regimes, which represent the three types of days described in the observations section. (1) A solar radiation–dominated regime accounts for 43 d, or approximately 88% of the record. Large or moderate heating events occurred during these days with significant variations in wind forcing, but stratification formation was dominated by the net heat flux, instead of wind mixing. (2) A windy regime was observed for 3 d, or 6% of the record. Lastly, (3) a cold inflow regime occurred for 3 d (6%) of the record. The empirically observed boundaries for these regimes are in terms of I_{IW} and I_{WB}: solar radiation–dominated regime, $I_{IW} < 0.4$ and $I_{WB} < 1$; windy regime, $I_{IW} < 0.4$ and $I_{WB} > 1$; cold inflow regime, $I_{IW} > 0.4$ and $I_{WB} < 1$.

It is observed that most of the days in the solar radiation–dominated regime are within the prediction bounds of the linear regression (Eq. 10) and that days in the cold inflow regime are beyond the upper bound, whereas days in the windy regime are below the lower bound of the linear regression fit. This is consistent with the physics of each of the regimes, i.e., vertical ΔT in the solar radiation regime can be largely determined by the solar radiation within a certain level of uncertainty; ΔT in the cold inflow regime is much larger than predicted by the solar radiation using Eq. 10, as plunging cold inflow increases the vertical stratification; whereas ΔT in the windy regime is much lower than predicted using Eq. 10, as stronger wind mixing reduces the vertical stratification formed by radiative heating.

However, there exist a few days close to the prediction bounds of the linear regression (*see* Fig. 9) as well as to the regime boundaries (*see* Fig. 10). To further determine the validity of the delineation of these days, specifically, DOYs 107, 119, 114, and 124, 15 min time series data of I_{WB} and I_{IW} during each of these 4 d are plotted in the I_{IW}–I_{WB} plane together with the boundaries of different regimes in Fig. 11. Seventy percent of the time series data during DOY 124 are within the upper left quadrant of the plot, which indicates that during most of the time in DOY 124 the stratification was dominated by wind mixing. Similarly, 100% of the time series data during DOY 114 are within the lower right quadrant of the plot, indicating that during DOY 114 wind mixing was always weak compared to inflow-induced stratification. Finally, for DOYs 107 and 119, 52% and 65%, respectively, of the time series data during these 2 d are within the lower left quadrant of the plot, i.e., the solar radiation–dominated regime. Thus, via this way of closer examination, the delineation of days close to the prediction bounds is validated.

In the solar radiation–dominated regime, the incoming solar radiation was large during the day and strong vertical stratification formed in the afternoon. For example, on DOY 110, $\overline{Q}_{sw} = 184$ W m^{-2} and $\Delta T_{\max} = 1.1^{\circ}$C, which was achieved late in the afternoon (*see* Fig. 5). The daily averaged $I_{WB} = 0.54$, so wind mixing effects were small for this case.

In the windy regime, strong winds during the day mixed the waters in the surface layer and deepened it. The stratification of the water column was dominated by the wind mixing instead of the net heat flux. Daily max ΔT in the windy regime was smaller than that in the solar radiation regime at comparable daily average solar radiation (*see* Fig. 9). For example, on DOYs 124 and 125, daily averaged I_{WB} was 1.43 and 1.45, respectively. The temperature field evolution in DOY 125 shown in Fig. 6D had a $\Delta T_{\max}$ of 0.6°C, whereas the $\overline{Q}_{sw}$ was

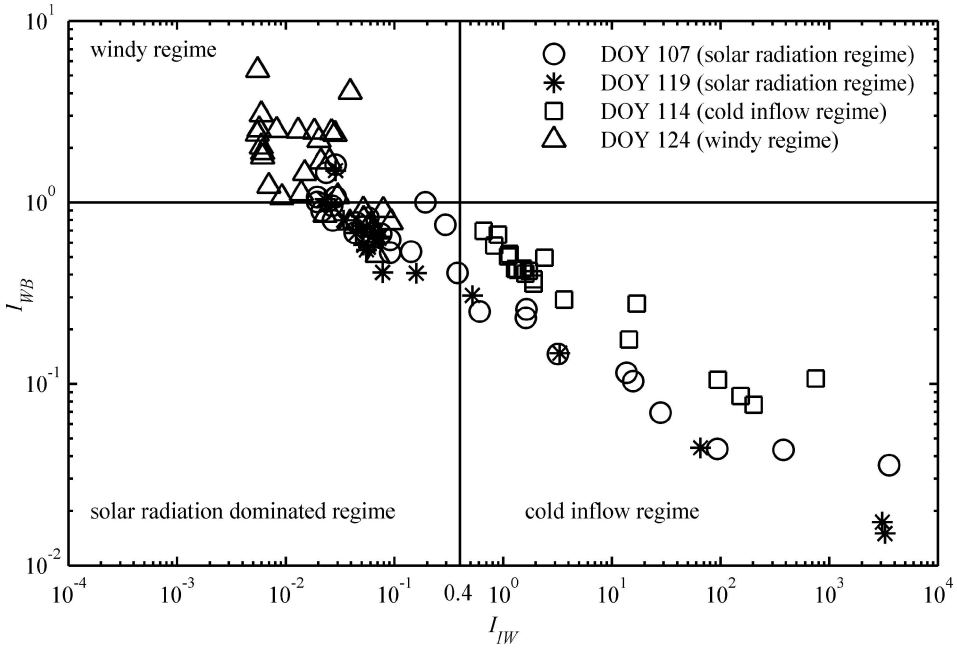

Fig. 11. Fifteen minute time series data of I_{WB} vs. I_{IW} on DOYs 107, 119, 114, and 124 in the I_{IW}–I_{WB} plane, which shows boundaries of different regimes.

175 W m^{-2}. In contrast, in the solar radiation regime a day at comparable $\overline{Q}_{sw}$ results in a $\Delta T_{\max}$ notably larger than 1°C (*see* Fig. 9).

In the cold inflow regime, appreciable cold inflow arising from large rainfall events plunged into the lower layers of the water column and increased the stratification. At comparable daily average solar radiation, $\Delta T_{\max}$ in the cold inflow regime was significantly greater than $\Delta T_{\max}$ in the solar radiation regime. On DOY 116, $\overline{Q}_{sw}$ was 91 W m^{-2} and there was a total of 36 mm of rainfall on the reservoir surface in the early morning (Fig. 7). On DOYs 116 and 117, daily averaged I_{IW} was 1.7 and 0.5, respectively, and $\Delta T_{\max}$ for these 2 d was significantly higher than for days in the solar radiation regime at comparable daily average solar radiation (Fig. 9).

The observations we report in this paper highlight the importance of diurnal and synoptic variability in mixing and heating, as well as the key role played by shallow regions and inflows in determining thermal structure and, thus, overall physics of such shallow tropical lakes. The dynamical balance of the system is sensitive to small forcing events, with the timescale of changes as short as a day or less, shorter than the estimated internal seiche period of 26.1 h. Strong stratification is formed if sufficient net solar radiation is available and is reduced almost every day in the reservoir by nighttime cooling. Analysis of the field deployment data indicates three dynamical regimes: a solar radiation–dominated regime, a windy regime, and a cold inflow regime; and these regimes are further delineated by two dimensionless numbers, I_{IW} and I_{WB}, with I_{WB} being similar to the Monin–Obukhov length (Imberger 1985). Most importantly, it appears that the usual conceptual model of lakes, in which they are viewed as having a background stratification that evolves seasonally and is perturbed by distinct forcing events (Imberger 1985), is inappropriate for shallow tropical systems like Kranji Reservoir. Traditional selective withdrawal might not be suitable for a shallow tropical reservoir like Kranji since there is no seasonal thermocline formed in the water column. Lastly, studies of phytoplankton dynamics and nutrients cycling vertically need to take into account the vertical mixing intensity and the short timescale of thermal (de)stratification cycles.

Acknowledgments

We are grateful to Public Utilities Board (PUB) of Singapore for providing access to the reservoir as well as logistical support during equipment deployment and retrieval. Liv Walter, Jonah Steinbuck from Stanford University, and the lab technicians of Hydraulics Laboratory of School of Civil and Environmental Engineering, Nanyang Technological University, were invaluable during the deployment and recovery of the field instruments. We also thank the reviewers for their comments, which improved the content and clarity of the paper. This research was sponsored by the Singapore Stanford Partnership program.

References

Antenucci, J. P., K. M. Tan, H. Eikass, and J. Imberger. 2013. The importance of transport processes and spatial gradients on in situ estimates of lake metabolism. Hydrobiologia **700:** 9–21, doi:10.1007/s10750-012-1212-z

Boon, P. J. 1996. The conservation of fresh waters: Temperate experience in a tropical context, p. 333–344. *In* F. Schiemer and K. T. Boland [eds.], Perspectives in tropical limnology. SPB Academic Publishing.

Cormack, D. E., L. G. Leal, and J. Imberger. 1974. Natural convection in a shallow cavity with differentially heated end walls. Part 1. Asymptotic theory. J. Fluid Mech. **65:** 209–230, doi:10.1017/S0022112074001352

Crisman, T. L., and W. J. Streever. 1996. The legacy and future of tropical limnology, p. 27–42. *In* F. Schiemer and K. T. Boland [eds.], Perspectives in tropical limnology. SPB Academic Publishing.

Fischer, H. B. 1976. Mixing and dispersion in estuaries. Annu. Rev. Fluid Mech. **8:** 107–133, doi:10.1146/annurev.fl.08.010176.000543

———, E. J. List, R. C. Y. Koh, J. Imberger, and N. H. Brooks. 1979. Mixing in inland and coastal waters. Academic Press.

Gin, K. Y.-H., and A. P. Gopalakrishnan. 2010. Sediment oxygen demand and nutrient fluxes for a tropical reservoir in Singapore. J. Environ. Eng. **136:** 78–85, doi:10.1061/(ASCE)EE.1943-7870.0000119

Gunkel, G., and J. Casallas. 2002. Limnology of an equatorial high mountain lake—Lago San Pablo, Ecuador: The significance of deep diurnal mixing for lake productivity. Limnologica **32:** 33–43, doi:10.1016/S0075-9511(02)80015-9

Hutchinson, G. E., and H. Löffler. 1956. The thermal classification of lakes. Proc. Natl. Acad. Sci. USA **42:** 84–86, doi:10.1073/pnas.42.2.84

Idso, S. B. 1973. On the concept of lake stability. Limnol. Oceanogr. **18:** 681–683, doi:10.4319/lo.1973.18.4.0681

Imberger, J. 1985. The diurnal mixed layer. Limnol. Oceanogr. **30:** 737–770, doi:10.4319/lo.1985.30.4.0737

———, and J. C. Patterson. 1990. Physical limnology. Adv. Appl. Mech. **27:** 303–475, doi:10.1016/S0065-2156(08)70199-6

Lewis, W. M., Jr. 1973. The thermal regime of Lake Lanao (Philippines) and its theoretical implications for tropical lakes. Limnol. Oceanogr. **18:** 200–217, doi:10.4319/lo.1973.18.2.0200

———. 1983. A revised classification of lakes based on mixing. Can. J. Fish. Aquat. Sci. **40:** 1779–1787, doi:10.1139/f83-207

———. 1987. Tropical limnology. Annu. Rev. Ecol. Syst. **18:** 159–184, doi:10.1146/annurev.es.18.110187.001111

———. 2000. Basis for the protection and management of tropical lakes. Lakes Reserv.: Res. Manage. **5:** 35–48.

MacIntyre, S., and J. M. Melack. 1995. Vertical and horizontal transport in lakes: Linking littoral, benthic, and pelagic habitats. J. North Am. Benthol. Soc. **14:** 599–615, doi:10.2307/1467544

———, J. R. Romero, and G. W. Kling. 2002. Spatial-temporal variability in mixed layer deepening and lateral advection in an embayment of Lake Victoria, East Africa. Limnol. Oceanogr. **47:** 656–671, doi:10.4319/lo.2002.47.3.0656

Monismith, S. G., J. Imberger, and M. L. Morison. 1990. Convective motions in the sidearm of a small reservoir. Limnol. Oceanogr. **35:** 1676–1702, doi:10.4319/lo.1990.35.8.1676

Nilssen, J. P. 1984. Tropical lakes—functional ecology and future development: The need for a process-orientated approach. Hydrobiologia **113:** 231–242, doi:10.1007/BF00026611

Parinet, B., A. Lhote, and B. Legube. 2004. Principal component analysis: An appropriate tool for water quality evaluation and management—application to a tropical lake system. Ecol. Model. **178:** 295–311, doi:10.1016/j.ecolmodel.2004.03.007

Pope, S. B. 2000. Turbulent flows. Cambridge Univ. Press.

Robertson, D. M., and J. Imberger. 1994. Lake number, a quantitative indicator of mixing used to estimate changes in dissolved oxygen. Int. Rev. Hydrobiol. (Int. Rev. Gesamten Hydrobiol.) **79:** 159–176, doi:10.1002/iroh.19940790202

Ruardij, P., H. V. Haren, and H. Ridderinkhof. 1997. The impact of thermal stratification on phytoplankton and nutrient dynamics in shelf seas: A model study. J. Sea Res. **38:** 311–331, doi:10.1016/S1385-1101(97)00042-7

Rueda, F. J., and S. G. Schladow. 2003. Dynamics of large polymictic lake. II: Numerical simulations. J. Hydraul. Eng. **129:** 92–101, doi:10.1061/(ASCE)0733-9429(2003)129:2(92)

———, ———, S. G. Monismith, and M. T. Stacey. 2003. Dynamics of large polymictic lake. I: Field observations. J. Hydraul. Eng. **129:** 82–91, doi:10.1061/(ASCE)0733-9429(2003)129:2(82)

Spigel, R. H., and J. Imberger. 1980. The classification of mixed-layer dynamics in lakes of small to medium size. J. Phys. Oceanogr. **10:** 1104–1121, doi:10.1175/1520-0485(1980)010<1104:TCOMLD>2.0.CO;2

Talling, J. F. 2001. Environmental controls on the functioning of shallow tropical lakes. Hydrobiologia **458:** 1–8, doi:10.1023/A:1013121522321

———, and J. Lemoalle. 1998. Ecological dynamics of tropical inland waters. Cambridge Univ. Press.

Tan, S. B. K., L. H. C. Chua, E. B. Shuy, E. Y.-M. Lo, and L. W. Lim. 2008. Performances of rainfall-runoff models calibrated over single and continuous storm flow events. J. Hydrol. Eng. **13:** 597–607, doi:10.1061/(ASCE)1084-0699(2008)13:7(597)

Xing, Z., D. A. Fong, K. M. Tan, E. Y.-M. Lo, and S. G. Monismith. 2012. Water and heat budgets of a shallow tropical reservoir. Water Resour. Res. **48:** W06532, doi:10.1029/2011WR11314

Associate editor: Chris Rehmann

Received: 17 March 2013
Accepted: 29 August 2013
Amended: 10 September 2013